Journal of Zhejiang University-SCIENCE B (Biomedicine & Biotechnology) *2022 23(4):300-314*
www.jzus.zju.edu.cn; www.springer.com/journal/11585
E-mail: jzus_b@zju.edu.cn

Research Article

https://doi.org/10.1631/jzus.B2100806

Check for updates

Comparative metabolomics provides novel insights into the basis of petiole color differences in celery (*Apium graveolens* L.)

Mengyao LI[1], Jie LI[1], Haohan TAN[1], Ya LUO[1], Yong ZHANG[1], Qing CHEN[1], Yan WANG[1,2], Yuanxiu LIN[1,2], Yunting ZHANG[1,2], Xiaorong WANG[1,2], Haoru TANG[1,2]✉

[1]*College of Horticulture, Sichuan Agricultural University, Chengdu 611130, China*
[2]*Institute of Pomology and Olericulture, Sichuan Agricultural University, Chengdu 611130, China*

Abstract: Plant metabolites are important for plant development and human health. Plants of celery (*Apium graveolens* L.) with different-colored petioles have been formed in the course of long-term evolution. However, the composition, content distribution, and mechanisms of accumulation of metabolites in different-colored petioles remain elusive. Using ultra-high performance liquid chromatography-tandem mass spectrometry (UHPLC-MS/MS), 1159 metabolites, including 100 lipids, 72 organic acids and derivatives, 83 phenylpropanoids and polyketides, and several alkaloids and terpenoids, were quantified in four celery cultivars, each with a different petiole color. There were significant differences in the types and contents of metabolites in celery with different-colored petioles, with the most striking difference between green celery and purple celery, followed by white celery and green celery. Annotated analysis of metabolic pathways showed that the metabolites of the different-colored petioles were significantly enriched in biosynthetic pathways such as anthocyanin, flavonoid, and chlorophyll pathways, suggesting that these metabolic pathways may play a key role in determining petiole color in celery. The content of chlorophyll in green celery was significantly higher than that in other celery cultivars, yellow celery was rich in carotenoids, and the content of anthocyanin in purple celery was significantly higher than that in the other celery cultivars. The color of the celery petioles was significantly correlated with the content of related metabolites. Among the four celery cultivars, the metabolites of the anthocyanin biosynthesis pathway were enriched in purple celery. The results of quantitative real-time polymerase chain reaction (qRT-PCR) suggested that the differential expression of the chalcone synthase (*CHS*) gene in the anthocyanin biosynthesis pathway might affect the biosynthesis of anthocyanin in celery. In addition, HPLC analysis revealed that cyanidin is the main pigment in purple celery. This study explored the differences in the types and contents of metabolites in celery cultivars with different-colored petioles and identified key substances for color formation. The results provide a theoretical basis and technical support for genetic improvement of celery petiole color.

Key words: Celery; Metabolite; Anthocyanin; Chlorophyll; Petiole color

1 Introduction

Celery (*Apium graveolens* L.), a biennial herb in the Family Apiaceae, is widely cultivated in the world. It is rich in protein, vitamins, dietary fiber, and other nutrients. It also contains numerous biologically active ingredients, such as apigenin, coumarin, anthocyanin, and volatile oil (Li et al., 2018). Apigenin is abundant in celery and has diverse pharmacological properties, including anti-inflammatory, antioxidative, and anti-bacterial properties, and the ability to lower blood pressure (Tan et al., 2017). Coumarin, another antioxidant in celery, can reduce cell canceration, and coumarin compounds can lower blood pressure and enhance the vascular system (Sowbhagya, 2014). Previous studies also found that celery is rich in volatile oil, which has potent effects on immunotoxicity and antioxidant activity (Nagella et al., 2012; Patil et al., 2015). Celery has high nutritional and medical values and is widely used in the food industry, medicine, and other fields.

Plant color is affected mainly by the content and distribution of pigments such as chlorophyll, carotenoids, and anthocyanins. Chlorophyll is composed of

✉ Haoru TANG, htang@sicau.edu.cn
Haoru TANG, https://orcid.org/0000-0001-6008-2747

Received Sept. 17, 2021; Revision accepted Dec. 14, 2021;
Crosschecked Mar. 1, 2022

© Zhejiang University Press 2022

chlorophyll a and chlorophyll b, providing green pigment (Wu et al., 2020). Carotenoids are the pigments responsible mainly for the yellow, red, and orange colors of diverse plants, such as carrots, corn, tomatoes, and pumpkins (Grotewold, 2006). Anthocyanins are a group of water-soluble plant pigments belonging to a flavonoid class of secondary metabolites synthesized by plants (Shi et al., 2020). For example, the purple sweet potato has a high content of anthocyanins that provide the characteristic purple color (Fenger et al., 2021). Carotenoids and anthocyanins are also crucial in plant growth and development, playing important roles in biological processes such as endogenous hormone biosynthesis (Xia et al., 2021), and enhancing tolerance to oxidation and drought stress (Nakabayashi et al., 2014). Plant pigments not only have the advantages of high safety and non-toxic side effects, but also have good health functions, including antioxidation and anti-aging properties and the ability to lower blood lipids, which are important factors for food quality (Ma et al., 2020).

Metabolomics involves mainly the global analysis of the dynamic regulation of small metabolic molecules and metabolic networks in organisms (Fiehn, 2002; Liu et al., 2020). Compared with traditional methods, metabolomics can rapidly screen out different substances among different samples, to better understand the mechanisms of biological phenomena. This novel technology has been widely used in nutrition, life sciences, and other fields. Metabolomics analysis was used to delineate the biochemical regulation underlying desiccation tolerance in *Sporobolus stapfianus* and reveal adaptive metabolic responses to dehydration (Oliver et al., 2011). At least 16 kinds of anthocyanins were identified in asparagus using metabolomics, revealing different mechanisms of stem color change (Dong et al., 2019). Zhang et al. (2020) found that different metabolic mechanisms in three maize cultivars resulted in different characteristics and quality.

The abundant metabolites in plants not only play an important role in their growth and development, but also are closely related to human health. In recent years, celery breeding research has developed rapidly, and important progress has been made in quality breeding, stress resistance breeding, and germplasm innovation. In particular, the breeding of celery cultivars with richer colors has attracted the attention of consumers. Although some metabolites in celery have been identified, systematic studies exploring the molecular mechanisms underlying differential metabolite accumulation in different celery cultivars are scarce. Herein, four celery cultivars with conspicuous colors (white, yellow, green, and purple) were used as plant materials to explore the metabolite components of petioles using untargeted metabolomics profile analysis. Differential metabolites were mined and metabolic pathways were clarified. Furthermore, anthocyanin accumulation and molecular analysis of correlated genes were investigated. This study provides information on the mechanisms of petiole color development in celery and promotes further improvement of celery quality or other characteristics through the analysis of specific metabolites.

2 Materials and methods

2.1 Plant materials and growing conditions

In this study, four celery cultivars, each with a different petiole color, were selected: "Baigu Huangxinqin" (HXQ, yellow petiole; Caiyuan Seed Shop, Guangzhou, China), "Gengyun Ziqin" (ZQ, purple petiole; Tianjin Gengyun Seed Industry Co., Ltd., Tianjin, China), "Gengyun Baoqin" (BQ, green petiole; Tianjin Gengyun Seed Industry Co., Ltd.), and "Xuebaiqin" (XBQ, white petiole; Shandong Fengpei Agricultural Technology Co., Ltd., Weifang, China). Seeds of each of the four celery cultivars were sown in a hole plate and put in an incubator at 20 °C and humidity of 80% to raise seedlings. When the seedlings grew 2−3 true leaves, they were moved into pots containing a nutrient soil/vermiculite/perlite mixture (3:1:1, volume ratio) for routine management. About 60 d later, each petiole sample was harvested, quick-frozen in liquid nitrogen, and stored in an ultra-low temperature refrigerator at −80 °C for later use.

2.2 Determination of chlorophyll and carotenoid contents

A solution of acetone-ethanol mixture (1:1, volume ratio) was used to extract chlorophyll and carotenoids. About 0.5 g of sample was added to 10 mL of extracting solution, placed at room temperature in darkness for 24 h, and shaken every hour until the material turned white. After centrifugation at 8000*g* at 25 °C for 5 min, the absorbance was measured at 470 (A_{470}),

645 (A_{645}), and 663 nm (A_{663}) wavelengths. The content (C, mg/g fresh weight (FW)) of each pigment in the material was calculated using the modified Arnon formulae:

$$C_{\text{chlorophyll a}} = 13.95 \times A_{663} - 6.88 \times A_{645}, \quad (1)$$

$$C_{\text{chlorophyll b}} = 24.96 \times A_{645} - 7.32 \times A_{663}, \quad (2)$$

$$C_{\text{chlorophyll}} = 20.20 \times A_{645} + 8.02 \times A_{663}, \quad (3)$$

$$C_{\text{carotenoid}} = 1000 \times A_{470} - 3.27 \times C_{\text{chlorophyll a}} - 104 \times C_{\text{chlorophyll b}}. \quad (4)$$

2.3 Determination of total anthocyanins

Total anthocyanin was extracted from the samples and analyzed as previously described (Wei et al., 2016). About 0.5 g of sample was added to 5 mL of 1% (volume fraction) hydrochloric acid (HCl) and methanol solution in a 15-mL centrifuge tube. After shaking, samples were placed in the dark at 4 ℃ for over 20 h, followed by ultrasonic treatment for 30 min at 4 ℃. After centrifugation at 8000*g* at 4 ℃ for 5 min, the absorbance of each sample was measured at 530, 620, and 650 nm.

2.4 Determination of anthocyanin components

About 2.0 g liquid nitrogen for grinding was added into 10 mL of extraction solution (95% ethanol: 1.5 mol/L HCl=85:15, volume ratio) and ultrasonically extracted for 30 min at 4 ℃. The samples were centrifuged at 5000*g* at 4 ℃ for 5 min. The supernatant was retained and the pellet was extracted again, and the supernatants were combined. About 5 mL of concentrated HCl was added to each sample, and the solution was incubated at 90 ℃ for 40 min. Acetonitrile (Thermo fisher, Shanghai, China) solution at a constant volume of 25 mL, 0.22-μm filtration membrane, and high-performance liquid chromatography (HPLC) were used for detection. The conditions for HPLC are as follows: chromatographic column was Poroshell 120 SB-C18 reversed-phase column (2.1 mm×150 mm, 2.7 μm; Agilent, Shanghai, China); chromatograph was Agilent 1260 II (Shanghai, China); reference standards include cyanidin (Solarbio, Beijing, China) and pelargonidin (Solarbio); column temperature was 35 ℃; mobile phase included solvent A water/0.1% formic acid (Kelong, Chengdu, China) and solvent B acetonitrile (A:B=3:7, elution volume ratio); elution gradient was equal gradient; the volume of elution injection was 2 μL.

2.5 Metabolomics analysis

2.5.1 Sample preparation

About 100 mg of each celery sample was ground in liquid nitrogen and about 500 μL of 80% (volume fraction) methanol aqueous solution was added, followed by vortexing and incubation in an ice bath for 5 min and centrifugation at 5000*g* and 4 ℃ for 20 min. The sample was diluted with mass spectrometry (MS)-grade water to a methanol concentration of 53% (volume fraction). The supernatant was collected after centrifugation and then analyzed using ultra-HPLC-tandem MS (UHPLC-MS/MS) (Want et al., 2013). The quality control (QC) sample consisted of samples of equal volume taken from each experimental sample and pooled to check the repeatability of the experiment.

2.5.2 Chromatographic and mass spectrometric conditions

UHPLC-MS/MS analysis was performed using a Vanquish UHPLC system (Thermo Fisher, Germany) coupled with an Orbitrap Q Exactive™ HF-X mass spectrometer (Thermo Fisher, Germany). Samples were injected into the C18 column (Hypesil Gold column, 100 mm×2.1 mm, 1.9 μm; Thermo Fisher, USA) using a 17-min linear gradient at a flow rate of 0.2 mL/min. The column temperature was set as 40 ℃. The eluents for the positive polarity mode were eluent A (0.1% formic acid in water) and eluent B (methanol), and the eluents for the negative polarity mode were eluent A (5 mmol/L ammonium acetate, pH=9.0) and eluent B (methanol). The gradient elution procedure was as follows: 0 min, 98% A+2% B; 1.5 min, 98% A+2% B; 12 min, 100% B; 14 min, 100% B; 14.1 min, 98% A+2% B; 17 min, 98% A+2% B. The mass spectrum scanning range was selected as mass-to-charge ratio (m/z) of 100–1500. The electrospray ionization (ESI) source was set as follows: spray voltage 3.2 kV; sheath gas flow rate 40 arb. (arb.=arbitrary units); auxiliary gas flow rate 10 arb.; capillary temperature 320 ℃. Polarity: positive; negative; MS/MS secondary scanning was data-dependent.

2.5.3 Data preprocessing

The original file (.raw) obtained from the spectrum detection was imported into Compound Discoverer 3.1 (CD3.1, Thermo Fisher Scientific, Texas, USA) search software for simple screening of parameters

such as retention time and *m*/*z*. Peak extraction was then performed according to the actual mass tolerance of 5 ppm (parts per million, $\times10^{-6}$), signal intensity tolerance of 30%, signal/noise ratio of 3, minimum intensity of 100 000, and retention time tolerance of 0.2 min. After obtaining the area of each characteristic peak, accurate qualitative and relative quantitative results were obtained using mzCloud (https://www.mzcloud.org), mzVault (Thermo Fisher Scientific), and MassList (http://www.maldi-msi.org/mass) databases. Statistical analyses were performed using the statistical software R (Version 3.4.3), Python (Version 2.7.6), and CentOS (Version 6.6).

2.5.4 Identification and screening of metabolites

metaX software (Wen et al., 2017) was used to reveal differences in metabolic patterns of different groups by principal component analysis (PCA) and partial least square-discriminant analysis (PLS-DA). The PLS-DA model is a model evaluation parameter obtained by 7-fold cross-validation (when the number of sample biological repetitions $n\leqslant3$, it is *k*-fold cross-validation, $k=2n$), which refers to the variable importance in the projection (VIP) of the first principal component of the PLS-DA model. Hierarchical cluster analysis (HCA, Euclidean distance) and metabolite correlation analysis were used to annotate the function and classification of the identified metabolites. The Kyoto Encyclopedia of Genes and Genomes (KEGG) (Masoudi-Nejad et al., 2007), Human Metabolome Database (HMDB) (Wishart et al., 2007), and Lipid Metabolites and Pathways Strategy (LIPID MAPS) (Cotter et al., 2006) databases were used to reveal the relationship between samples and between metabolites. Differentially accumulated metabolites were screened out with selection criteria set as VIP>1.000, fold change (FC)>1.500 or <0.667, and $P<0.05$.

$$P=1-\sum_{j=0}^{X-1}\frac{\binom{M}{j}\binom{N-M}{n-j}}{\binom{N}{n}}, \tag{5}$$

where N is the background metabolite set, n is the differential metabolite set, M is the metabolites of a certain pathway, j is the differential metabolites of a certain pathway, and X is the number of differential metabolites enriched in a KEGG pathway.

2.5.5 Metabolic pathway analysis

The main biological functions of different metabolites were determined using the KEGG pathway enrichment analysis. The *P*-value of pathway enrichment was obtained using the hypergeometric test method. A *P*-value of ⩽0.05 was used as the threshold value to define a KEGG pathway that was significantly enriched in different metabolites.

2.6 qRT-PCR analysis

Quantitative real-time polymerase chain reaction (qRT-PCR) was performed using a CFX96TM real-time system (Bio-Rad, California, USA) with SYBR qPCR Master Mix Kit (Vazyme Biotech Co., Nanjing, China). Primers were designed by Primer Premier 6.0 software, and the primer sequences were listed in Table S1. *TUB* was used as an internal reference to normalize gene expression (Feng et al., 2019), and the relative gene expression was calculated by $2^{-\Delta\Delta C_T}$ (Pfaffl, 2001).

3 Results

3.1 Phenotypes and pigment contents of celery cultivars

Visual inspection of celery cultivars showed that HXQ, ZQ, BQ, and XBQ were significantly different in petiole color, with yellow, white, green, and purple colors, respectively (Figs. 1a and 1b). The contents of chlorophyll, carotenoids, and total anthocyanins in the four celery cultivars were determined (Fig. 1c). The results showed that the contents of chlorophyll and carotenoids in BQ and HXQ were significantly higher than those in ZQ and XBQ. The chlorophyll content was the highest in BQ, which has a deep green petiole. Chlorophyll and carotenoids were found in HXQ, but their contents were significantly lower than those in BQ. The highest level of anthocyanin accumulation was detected in ZQ, while the content of each of the three pigments was very low in XBQ.

3.2 Metabolomic profiles and statistical analysis

In the positive and negative ion modes, there was no drift in the total ion chromatogram of the QC

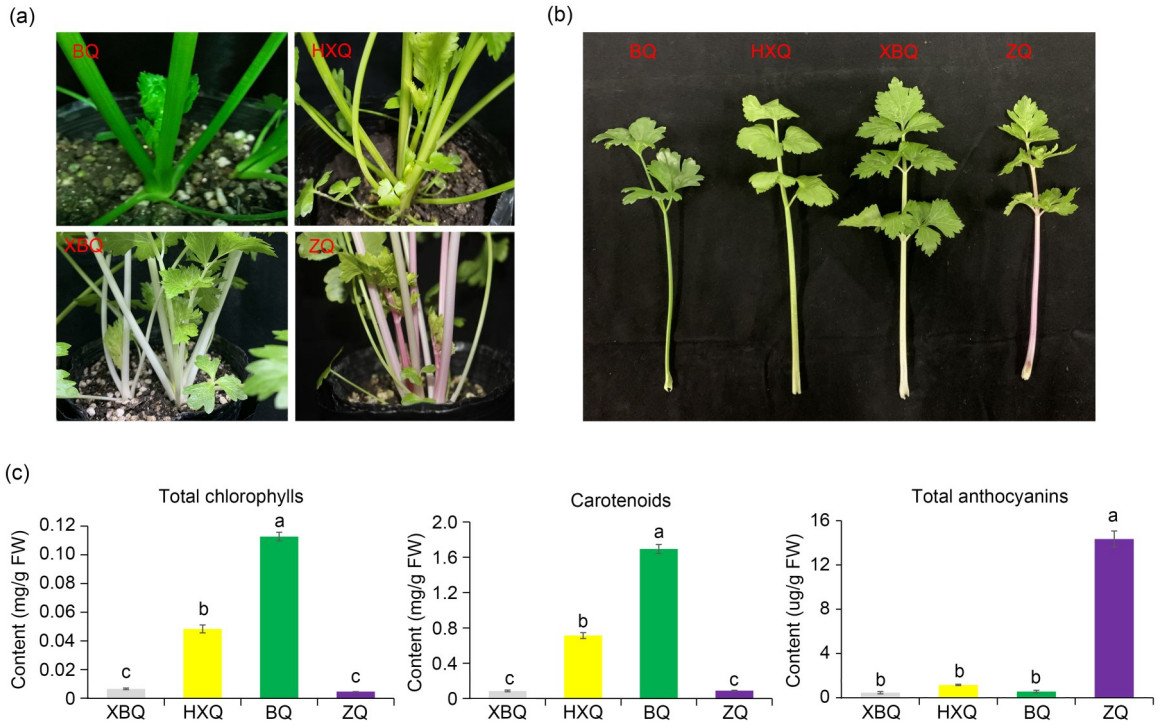

Fig. 1 Phenotypes (a, b) and pigment contents (c) in celery cultivars XBQ, HXQ, BQ, and ZQ. The contents of total chlorophylls, carotenoids, and total anthocyanins in petioles from the four cultivars are shown as mean±SD (*n*=3). Different letters on the vertical bars indicate a significant difference at *P*=0.05. BQ: Gengyun Baoqin, green petiole; HXQ: Baigu Huangxinqin, yellow petiole; XBQ: Xuebaiqin, white petiole; ZQ: Gengyun Ziqin, purple petiole; SD: standard deviation; FW: fresh weight.

sample (Fig. S1). Therefore, the metabolites and quantitative analysis results obtained were accurate and reliable. PCA was used to analyze the data in the positive and negative ion modes (Fig. S2). The QC samples were used for quality control detection. The distribution of QC samples in the PCA analysis map gathered together and the metabolites of the four groups showed a trend of separation and aggregation among groups, indicating that the data had good reproducibility during the experiment, and there were significant differences among the four celery cultivars.

A total of 1159 metabolites were detected in the four celery samples (Table S2), and were annotated using HMDB and LIPID MAPS classifications. Based on the HMDB, 420 metabolites were classified into 12 classes. The most frequently represented classes included "lipids and lipid-like molecules" (100 metabolites), "phenylpropanoids and polyketides" (83 metabolites), and "organic acids and derivatives" (72 metabolites) (Fig. 2a). Of the metabolites listed in Fig. 2b, "glycerophospholipids (GP)" represents one of the largest lipid families, but "flavonoids" was the main class with the most metabolites in the LIPID MAPS database.

3.3 Identification of differentially accumulated metabolites

To identify the metabolites associated with petiole color, a threshold for VIP of >1.0, FC>1.500 or <0.667, and a *P*-value of <0.05 were used to screen significant differences in metabolite accumulation. A total of 647 metabolites were differentially accumulated at least on pairwise comparisons, and the metabolites of the four celery cultivars were significantly different (Fig. 3a). The number of differentially accumulated metabolites was highest in BQ vs. ZQ with 335 metabolites (221 up-regulated and 114 down-regulated), followed by XBQ vs. BQ with 304 metabolites, and XBQ vs. ZQ with 233 metabolites. Except for HXQ vs. BQ, more metabolites were up-regulated in all pairwise comparisons, suggesting that most metabolites exhibited higher levels in BQ and XBQ. The ten most differentially up-regulated and down-regulated metabolites in each pairwise comparison are shown

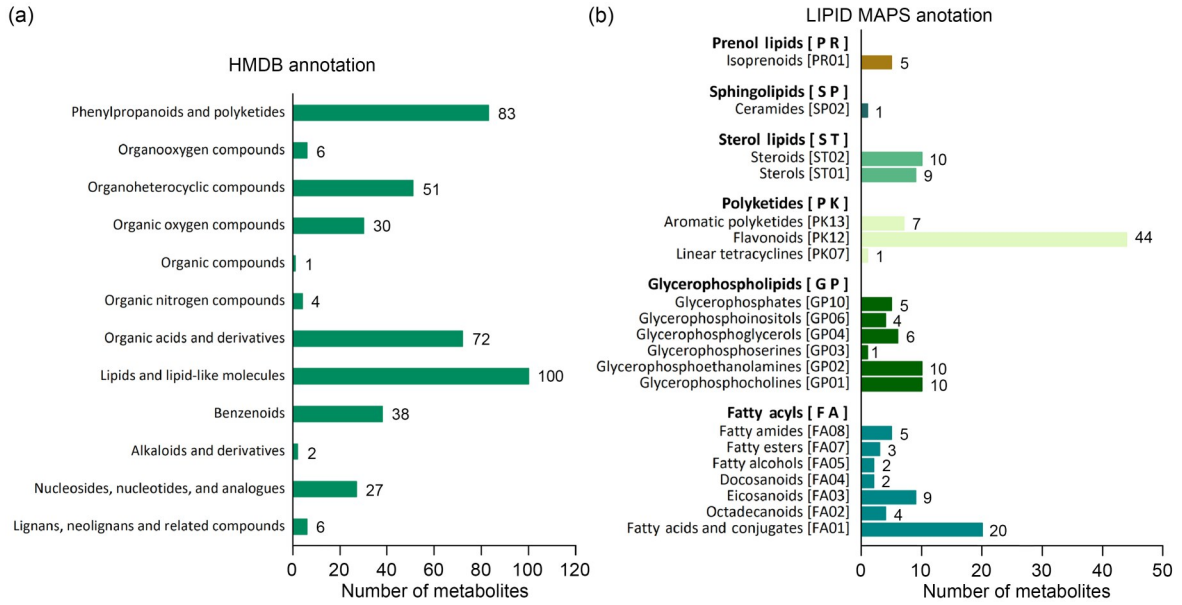

Fig. 2 Classification of metabolites according to annotation by HMDB (a) and LIPID MAPS database (b). HMDB: Human Metabolome Database; LIPID MAPS: Lipid Metabolites and Pathways Strategy.

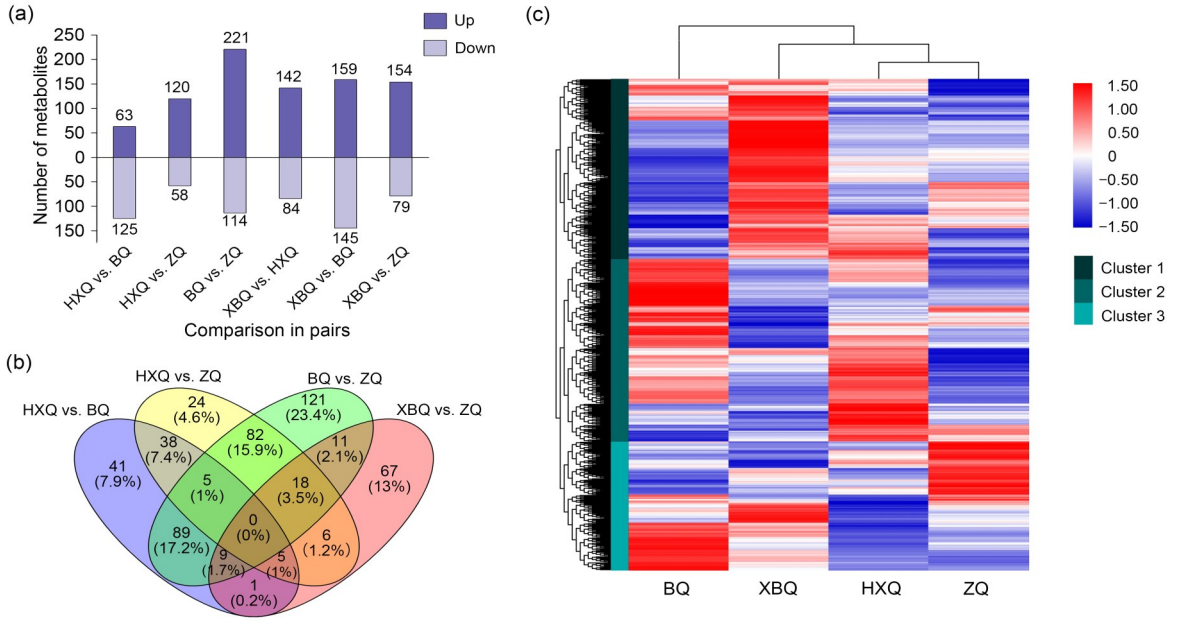

Fig. 3 Identification of differentially accumulated metabolites among four celery cultivars. (a) The number of differentially accumulated metabolites in any two celery cultivar. Up stands for up-regulation of metabolites and Down stands for down-regulation of metabolites. (b) Venn diagram of differentially accumulated metabolites shared or uniquely expressed in two or more comparisons. (c) Hierarchical clustering analysis of differential metabolite expression for all samples. The logarithmic quantitative results of metabolites are row scale. BQ: Gengyun Baoqin, green petiole; HXQ: Baigu Huangxinqin, yellow petiole; XBQ: Xuebaiqin, white petiole; ZQ: Gengyun Ziqin, purple petiole.

in Table S3. Some bioactive constituents such as quercetin, apigenin, and catechin were significantly different among the four cultivars. The highest apigenin content was found in HXQ, which was about 30 times higher than that in ZQ. BQ and XBQ had a high catechin content, whereas ZQ and HXQ maintained lower levels.

Four pairwise comparisons (HXQ vs. BQ, XBQ vs. ZQ, BQ vs. ZQ, and HXQ vs. ZQ) were further selected to analyze metabolites shared or uniquely

expressed in two or more comparisons (Fig. 3b). Some metabolites were significantly different only in one pairwise comparison, with 121 differentially accumulated metabolites exclusively present in BQ vs. ZQ, followed by 67 in XBQ vs. ZQ. A total of 89 differentially accumulated metabolites overlapped in HXQ vs. BQ and BQ vs. ZQ, while 82 were common in BQ vs. ZQ and HXQ vs. ZQ. The hierarchical clustering analysis of 647 different metabolites in the four celery cultivars showed a clear grouping pattern (Fig. 3c and Table S4), and all these metabolites were divided into three clusters. The trend observed in Fig. 3a was confirmed when the expression levels of metabolites were clustered: the most significantly up-regulated metabolites (red) were observed in BQ and XBQ, while the most down-regulated metabolites (blue) were observed in ZQ. However, the metabolites related to the anthocyanin biosynthesis pathway, such as quercetin, coumarin, cyanidin, kaempferide, and cinnamic acid, gathered in the third cluster and exhibited higher levels.

3.4 Metabolite–metabolite correlation analysis

To understand the correlation between metabolites of different samples, Pearson's correlation coefficients of all metabolites in each combination were calculated. A *P*-value of <0.05 was chosen as the threshold for significant correlation. Metabolites correlated with the 20 smallest *P*-values are shown in Fig. 4. Most correlations between metabolites in HXQ vs. BQ and HXQ vs. ZQ were positive, while most in the other four

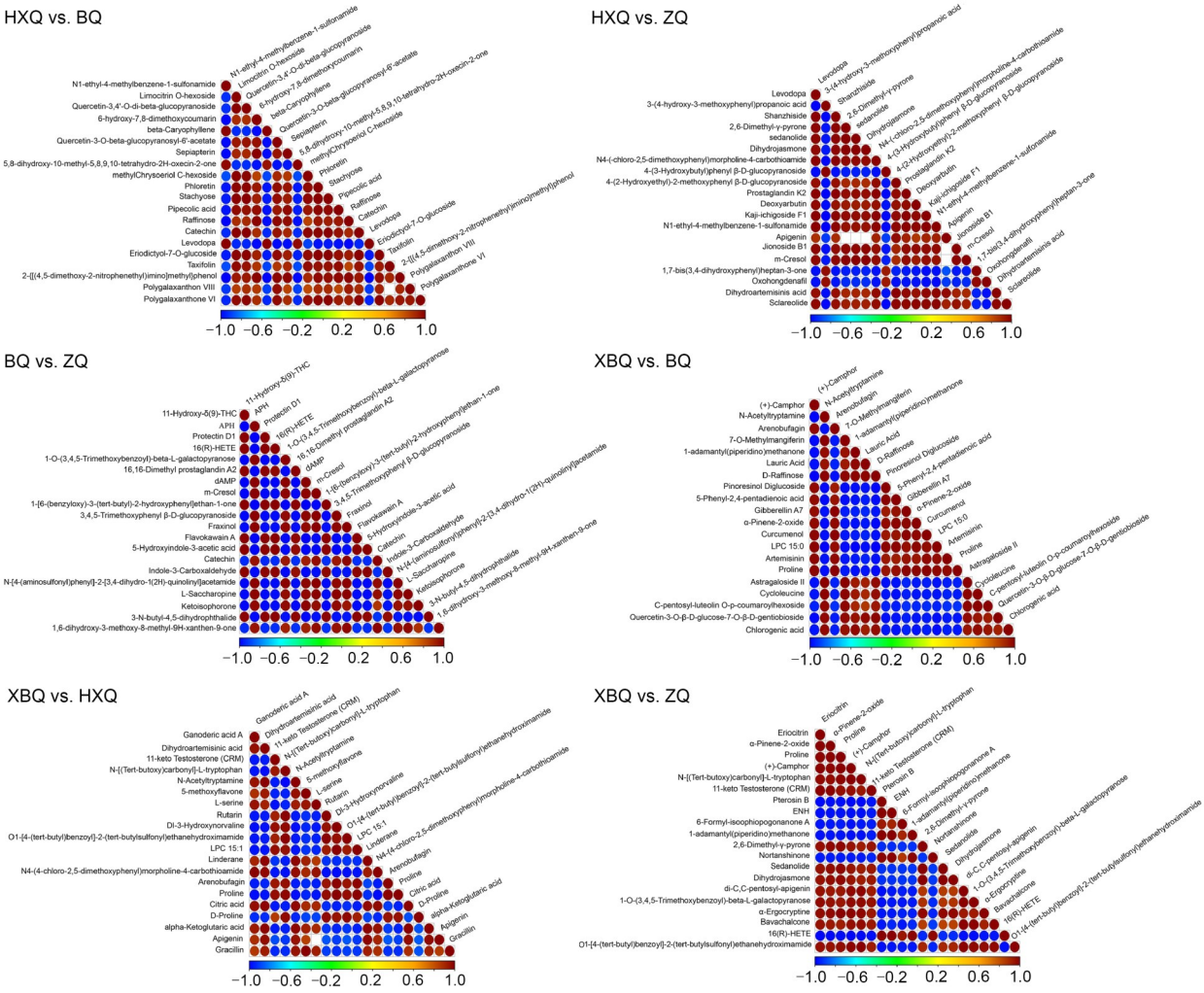

Fig. 4 Correlation analysis of the different metabolites in each pairwise comparison. The red and blue dots represent positive and negative correlations, respectively. The color scale represents Pearson's correlation coefficients. BQ: Gengyun Baoqin, green petiole; HXQ: Baigu Huangxinqin, yellow petiole; XBQ: Xuebaiqin, white petiole; ZQ: Gengyun Ziqin, purple petiole.

pairwise comparisons were negative. Flavonoids and lipids were mostly negatively correlated, while organic acids were mostly positively correlated. For example, catechin was negatively correlated with several lipids such as protectin D1, 16(*R*)-hydroxyeicosatetraenoic acid (HETE), and β-caryophyllene, and positively correlated with L-saccharopine and pipecolic acid. Curcumenol was significantly negatively correlated with lauric acid and significantly positively correlated with proline. In addition, apigenin, a flavonoid with good health effects, was significantly positively correlated with organic acids such as citric acid, α-ketoglutaric acid, and levodopa.

3.5 Metabolic pathway analyses of the differentially accumulated metabolites

The metabolic pathways of the differentially accumulated metabolites were analyzed based on the KEGG database. The results showed that the pathways enriched among different combinations were significantly different (Fig. 5). "Biosynthesis of secondary metabolites" was one of the most enriched pathways observed in all comparisons, especially in XBQ vs. BQ and HXQ vs. BQ. Except for XBQ vs. HXQ, most metabolites were significantly enriched in "flavonoid biosynthesis," while "phenylpropanoid biosynthesis" was found in five comparisons, except in HXQ vs. ZQ. Several metabolic pathways related to "isoflavonoid biosynthesis," "flavone and flavonol biosynthesis," and "stilbenoid, diarylheptanoid and gingerol biosynthesis" were also found to be significantly enriched. "Porphyrin and chlorophyll metabolism" was highly enriched in XBQ vs. BQ and BQ vs. ZQ, suggesting that chlorophyll may be related to the green color of celery. In addition, metabolites associated with anthocyanin synthesis were highly enriched in BQ vs. ZQ and HXQ vs. ZQ, which suggested that anthocyanins may be related to the purple color of celery.

3.6 Analyses of the expression of metabolites related to the chlorophyll biosynthesis pathway and qRT-PCR validation

By analyzing the metabolic pathways related to chlorophyll, we found that the metabolite contributing to the green color might be chlorophyll. By analyzing the chlorophyll pathway (Fig. 6a and Table S5), four metabolites related to chlorophyll synthesis and degradation were differentially expressed in the four celery cultivars. In particular, the accumulation of chlorophyll a and pheophorbide a in BQ was about twice that of HXQ and more than 20 times that of XBQ and ZQ. This result was roughly consistent with that of Fig. 1. Related enzyme encoding genes were found according to the chlorophyll synthesis pathway. qRT-PCR analysis showed that glutamyl-transfer RNA (tRNA) reductase (*HEMA*), chlorophyll a synthase (*CHLG*), pheophytinase (*PPH*), and pheophorbide a oxygenase (*PAO*) were expressed in all four celery cultivars (Fig. 6b); however, as anticipated, the expression levels of these genes in the green cultivar were significantly higher than those in the other three cultivars. The accumulation of metabolites was consistent with the genes, confirming that the greenish compound was chlorophyll.

3.7 Analysis of metabolite accumulation associated with the anthocyanin biosynthesis pathway

Because the anthocyanin synthesis pathway was enriched in differentially accumulated metabolites, the levels of accumulation of anthocyanin metabolites were estimated. A total of 20 metabolites were found to be related to anthocyanin synthesis (Fig. 7 and Table S5), and the expression levels of 14 metabolites were significantly different in the four celery cultivars. Among them, five metabolites (cinnamic acid, esculetin, naringenin, eriodictyol, and cyanidin) accumulated significantly in purple celery. As one of the main components of anthocyanin, the accumulation of cyanidin in ZQ was more than 10 times that of XBQ and HXQ, and about 6 times that of BQ. We speculated that cyanidin may be the main coloring substance of purple celery. In addition, several metabolites, including apigenin, coumarin, quercetin, and catechin, were highly expressed in different celery cultivars, which may be related to their participation in the synthesis of other substances. For example, apigenin was highly expressed in HXQ and BQ.

Differences in the proportion of anthocyanin among the different celery cultivars were further analyzed by the HPLC-MS/MS system. Reference standards of cyanidin and pelargonidin were used to compare the peaks. The results showed that only cyanidin was detected in ZQ (Fig. 8), whereas no anthocyanin component was detected in other celery samples.

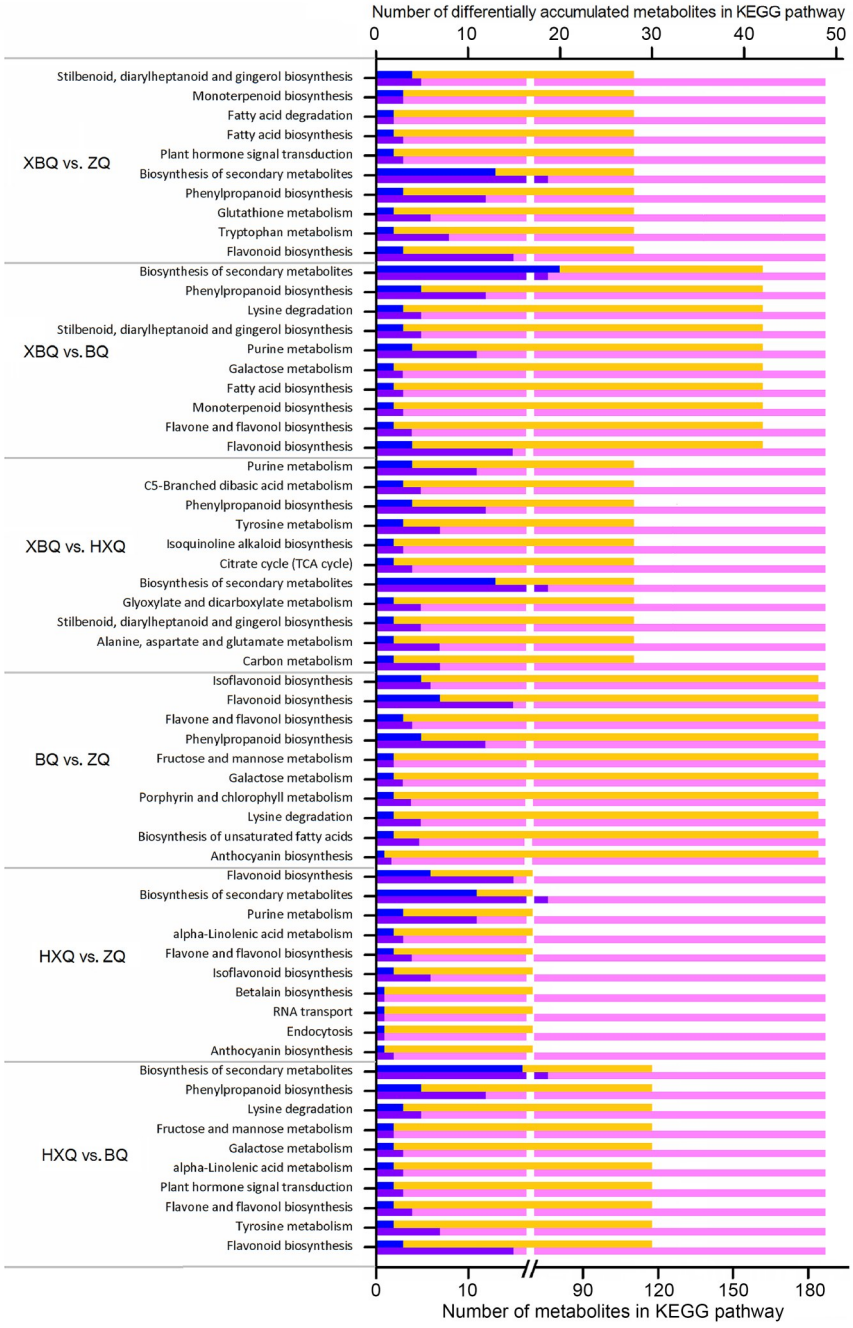

Fig. 5 Top 10 enrichment KEGG pathways. Blue bars represent the proportion of differentially accumulated metabolites related to each pathway in all differentially accumulated metabolites; orange bars represent all differential metabolites in each pathway; purple bars represent the proportion of metabolites related to each pathway in all metabolites obtained in this study; pink bars represent all the metabolites of each pathway. KEGG: Kyoto Encyclopedia of Genes and Genomes; BQ: Gengyun Baoqin, green petiole; HXQ: Baigu Huangxinqin, yellow petiole; XBQ: Xuebaiqin, white petiole; ZQ: Gengyun Ziqin, purple petiole.

3.8 Identification of the genes associated with anthocyanin biosynthesis pathway

qRT-PCR was performed to analyze the messenger RNA (mRNA) levels to unveil the roles of genes involved in anthocyanin accumulation. All 11 genes considerably correlated with anthocyanin synthesis were expressed in the samples (Fig. 9). As anticipated, the expression of most of the genes in the purple cultivar was significantly higher than that of those in the other

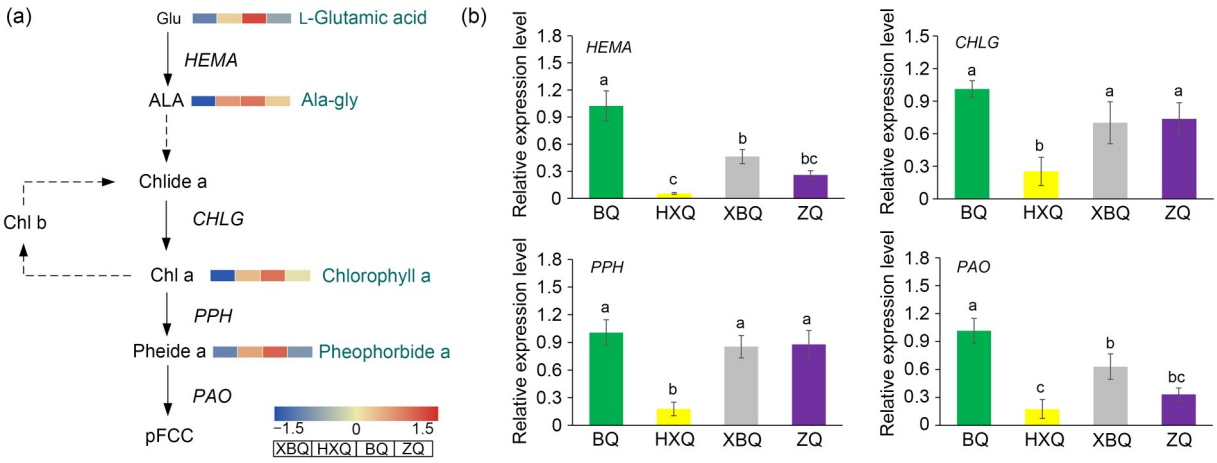

Fig. 6 Chlorophyll synthesis pathway in the four celery cultivars with different colors. (a) Metabolite expression levels of four samples are shown by heatmap, and the logarithmic quantitative results of metabolites are row scale; (b) qRT-PCR analyses of the expression levels of genes are shown as mean±SD of three biological replicates. Different letters on the vertical bars indicate a significant difference at P=0.05. Glu: L-glutamic acid; ALA: δ-aminolevulinic acid; Chlide a: chlorophyllide a; Chl a: chlorophyll a; Pheide a: pheophorbide a; pFCC: primary fluorescent chlorophyll metabolite; *PAO*: pheophorbide a oxygenase; *PPH*: pheophytinase; *CHLG*: chlorophyll a synthase; *HEMA*: glutamyl-transfer RNA (tRNA) reductase; BQ: Gengyun Baoqin, green petiole; HXQ: Baigu Huangxinqin, yellow petiole; XBQ: Xuebaiqin, white petiole; ZQ: Gengyun Ziqin, purple petiole; qRT-PCR: quantitative real-time PCR; SD: standard deviation.

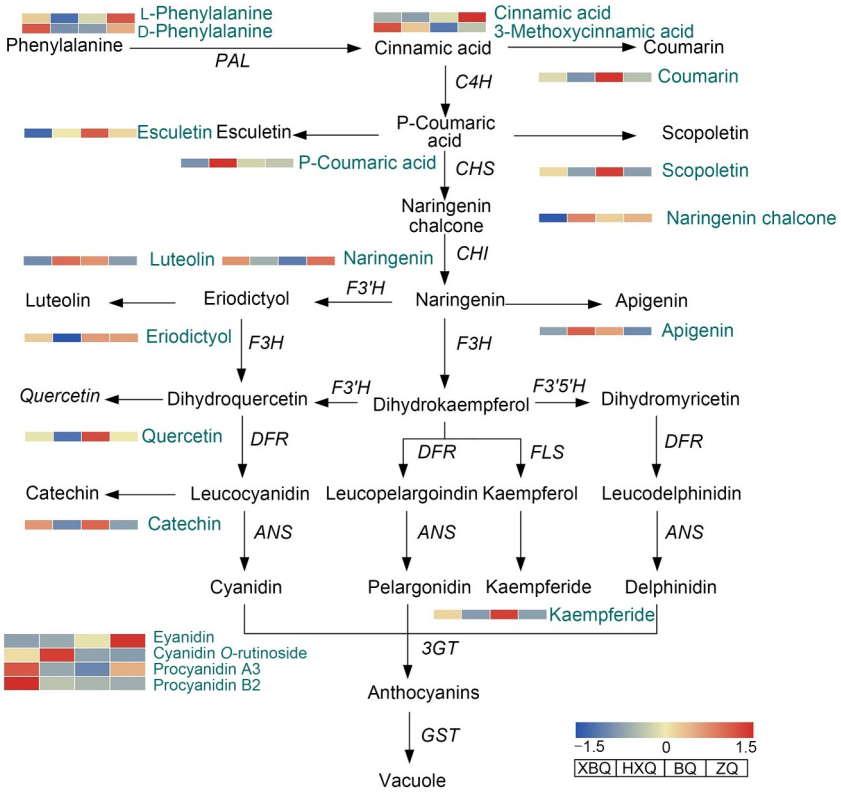

Fig. 7 Anthocyanin synthesis pathway in the four celery cultivars with different colors. The expression levels of metabolites in four samples are shown by heatmap. The metabolite logarithmic quantitative results are row scale. *PAL*: phenylalanine ammonia-lyase; *C4H*: cinnamic acid-4-hydroxylase; *CHS*: chalcone synthase; *CHI*: chalconeisomerise; *F3'H*: flavanone-3'-hydroxylase; *F3H*: flavanone-3-hydroxylase; *F3'5'H*: flavonoid-3',5'-hydroxylase; *DFR*: dihydroflavonol-4-reductase; *FLS*: flavonol synthase; *ANS*: anthocyanidin synthase; *3GT*: flavonoid-3-*O*-glucosyl-transferase; *GST*: glutathione *S*-transferase; BQ: Gengyun Baoqin, green petiole; HXQ: Baigu Huangxinqin, yellow petiole; XBQ: Xuebaiqin, white petiole; ZQ: Gengyun Ziqin, purple petiole.

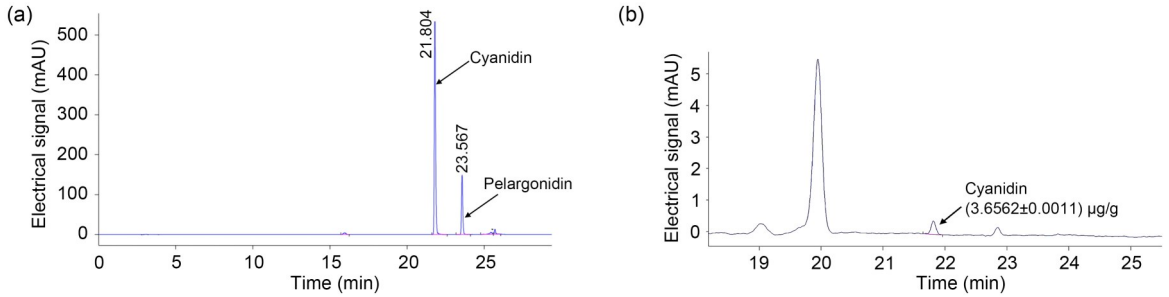

Fig. 8 HPLC analysis of the anthocyanin components. (a) HPLC chromatogram showing peaks for standard cyanidin. (b) HPLC chromatogram showing peak for cyanidin in ZQ. HPLC: high-performance liquid chromatography; ZQ: Gengyun Ziqin, purple petiole.

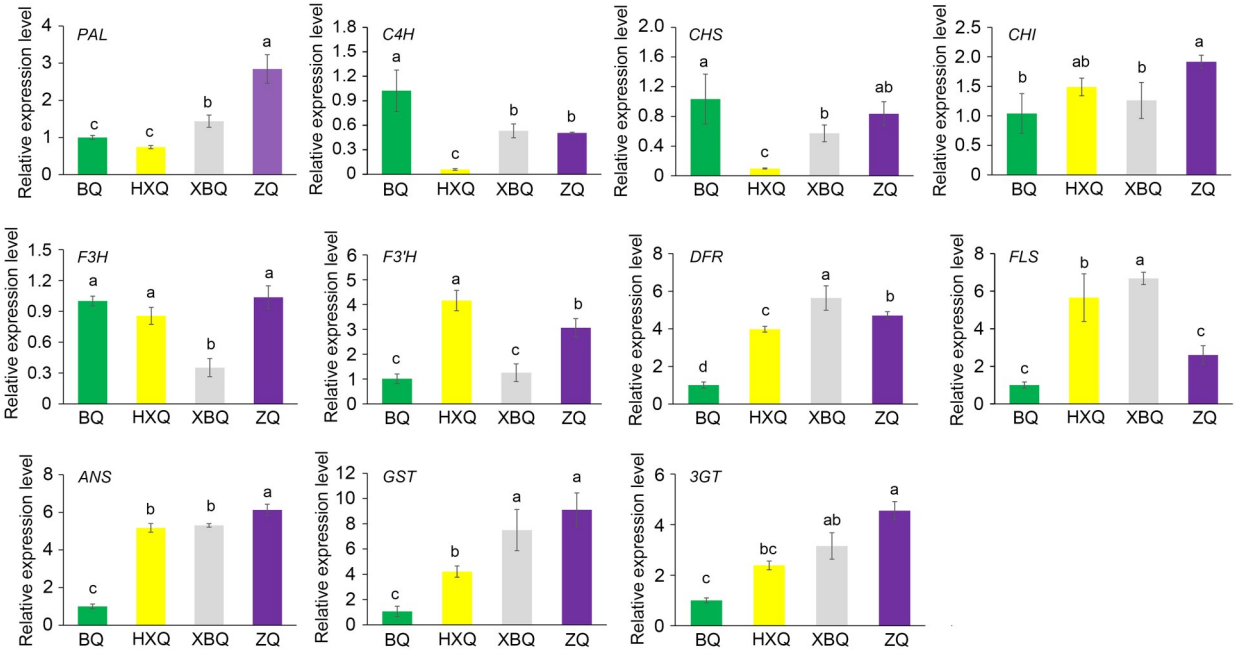

Fig. 9 qRT-PCR analyses of the expression levels of genes correlated with anthocyanin in four celery cultivars of different colors. Data are shown as mean±SD of three biological replicates. Different letters on the vertical bars indicate a significant difference at *P*=0.05. *PAL*: phenylalanine ammonia-lyase; *C4H*: cinnamic acid-4-hydroxylase; *CHS*: chalcone synthase; *CHI*: chalconeisomerise; *F3H*: flavanone-3-hydroxylase; *F3'H*: flavanone 3'-hydroxylase; *DFR*: dihydroflavonol-4-reductase; *FLS*: flavonol synthase; *ANS*: anthocyanidin synthase; *GST*: glutathione *S*-transferase; *3GT*: flavonoid-3-*O*-glucosyl-transferase; BQ: Gengyun Baoqin, green petiole; HXQ: Baigu Huangxinqin, yellow petiole; XBQ: Xuebaiqin, white petiole; ZQ: Gengyun Ziqin, purple petiole; qRT-PCR: quantitative real-time polymerase chain reaction; SD: standard deviation.

three cultivars. As the first key enzyme gene in the anthocyanin biosynthesis pathway, the expression level of phenylalanine ammonia-lyase (*PAL*) in purple celery was about three times higher than that in the other cultivars. Chalconeisomerise (*CHI*), anthocyanidin synthase (*ANS*), glutathione *S*-transferase (*GST*), and flavonoid-3-*O*-glucosyl-transferase (*3GT*) were most abundant in the purple celery and showed the highest expression, whereas they were lowly expressed in the green celery. In addition, chalcone synthase (*CHS*), flavanone-3-hydroxylase (*F3H*), dihydro fl avonol-4-reductase (*DFR*), and flavanone-3'-hydroxylase (*F3'H*) were relatively highly expressed in purple celery. Notably, metabolites such as cinnamic acid, naringenin chalcone, naringenin, eriodictyol, and cyanidin were significantly accumulated in purple celery. Metabolite accumulation was highly consistent with the expression trend of the genes, especially in the cyanidin synthesis pathway, suggesting that cyanidin was responsible for purple color of the celery petioles.

4 Discussion

Metabolites produced by organisms are generally believed to confer signals reflecting genetic structure and environmental adaptability (Jewett et al., 2006). Metabolomics, which can effectively help explore a series of metabolites produced by organisms in the process of life, is viewed as a bridge between genotypes and phenotypes (Fiehn, 2002; Zhang et al., 2019). The biosynthesis and accumulation of some plant metabolites, including chlorophyll, carotenoids, anthocyanins, and betaine, have a decisive influence on the color of plant tissues (Wang M et al., 2020; Jia et al., 2021; Li XB et al., 2021). However, the regulation of plant color is a complex process. Although multiple techniques such as omics and molecular biology have been used to study the mechanism of color formation of celery (Tan et al., 2017; Song et al., 2021), the synthesis and regulation mechanism of small-molecule metabolites in pigment accumulation in celery petioles remains elusive. In the present study, four celery cultivars with distinct colors were selected for comparative analysis. The contents of chlorophyll, carotenoids, and anthocyanin were significantly different. Green celery had a significantly higher chlorophyll content. Although there are numerous carotenoids in green celery, the green color of the chloroplast may conceal the yellow color (Sun et al., 2018). Yellow celery contains chlorophyll and carotenoids, but the contents are significantly lower than those of the green celery, which contributed to a phenotype with a deficiency of chlorophyll. White celery had very low contents of all three pigments, whereas the content of total anthocyanin in the purple celery was the highest. To explore the metabolites and related genes responsible for color diversity, we performed a metabolomics analysis of the four celery cultivars with diverse colors. A total of 1159 metabolites, including lipids, organic acids, phenylpropanoids, polyketides, and sugars, were detected in the petioles. Differentially accumulated metabolites were identified by conducting pairwise comparisons of the four celery cultivars. A total of 335 metabolites significantly differentiated between purple and green celery. Enrichment analysis revealed that these metabolites were enriched mainly in flavonoid biosynthesis, isoflavonoid biosynthesis, phenylpropanoid biosynthesis, anthocyanin biosynthesis, and porphyrin and chlorophyll metabolism.

Plant chlorophyll exists in several forms in vivo (Jiang et al., 2010). Chlorophyll provides energy for plants through photosynthesis, but excessive chlorophyll induces increased production of free radicals in plants, which may cause injury to plant cells. Chlorophyll degradation products can maintain cell activity. It is physiologically important for chlorophyll to be degraded in a timely way (Eckhardt et al., 2004). Pheophorbide is one of the main metabolites of chlorophyll degradation. In our study, chlorophyll a and pheophorbide were significantly higher in green celery than in the other cultivars, suggesting that synthesis and degradation of chlorophyll in the green celery exist in equilibrium. HEMA is the first enzyme of the chlorophyll biosynthesis pathway and catalyzes the transformation of L-glutamic acid (Glu) to δ-aminolevulinic acid (ALA) (Beale, 2005). In rice and grass, high expression of *HEMA* and *CHLG* promotes green coloration by increasing the chlorophyll content of the leaves (Zeng et al., 2020; Zhu et al., 2020). Significant up-regulation of genes related to chlorophyll metabolism was detected in the green celery compared with the other cultivars, suggesting that chlorophyll metabolic pathways might be the main pathways used to generate the green color pigments.

Differentially accumulated metabolites related to anthocyanin synthesis were detected at higher levels in the purple celery than in the other three celery cultivars, suggesting that differences in anthocyanin content are the main cause of purple celery color. Tan et al. (2017) also reported that the phenotype of purple celery was related to the anthocyanin synthesis pathway. Anthocyanin pigments such as cyanidin, pelargonidin, petunidin, and malvidin are responsible for the purple, blue, pink, and other deep-colored pigments of plant tissues (Liu et al., 2018; Han et al., 2021). Anthocyanin biosynthesis depends on several key enzymes encoded by early flavonoid biosynthesis genes (such as *PAL*, *CHS*, *CHI*, and *F3H*) and late biosynthetic genes (such as *DFR*, *ANS*, and uridine diphosphate (UDP)-glucose:flavonoid 3-*O*-glycosyltransferase (*UFGT*)). The structural genes encoding these enzymes have been studied in numerous species, including kiwifruit, pear, and carrot (Liu et al., 2019; Peng et al., 2019; Xu et al., 2020).

Tissue color is known to be correlated with the expression of genes related to anthocyanin synthesis. *PAL* and *ANS* genes play important roles in regulating

the biosynthesis of anthocyanins (Zhou et al., 2020). Of the 11 genes significantly correlated with anthocyanin content, eight were consistently up-regulated in the purple celery, especially *PAL* and *ANS*. As one of the key enzymes, the *PAL* gene was significantly expressed in the purple celery, which is conducive to the accumulation of a large amount of cinnamic acid. Phenylalanine, as the upstream reactant of anthocyanins and other flavonoids, is first converted to cinnamic acid under the catalysis of PAL (Ferreyra et al., 2012). Cinnamic acid is transformed into naringenin under the action of C4H, CHS, and CHI (Li SP et al., 2021). Afterward, different enzymes (F3H, F3'H, FLS, ANS, and other enzymes) catalyze naringenin via different pathways that are responsible for the synthesis of diverse classes of flavonoids (Jan et al., 2021). In the current study, *p*-coumaric acid, naringin, cinnamic acid, cyanidin, and other metabolites related to anthocyanin synthesis in the purple celery accumulated significantly and showed a strong positive correlation. The accumulation of metabolites was consistent with the gene expression results, suggesting that cyanidins were the most abundant anthocyanin substances in the purple celery.

Studies have shown that carotenoids are not the only source of the yellow color, and the significant expression of related genes in the anthocyanin synthesis pathway also makes plant tissues appear yellow. *PAL* and *CHS* are the main genes regulating the upstream of the yellow regulatory network in the cucumber pericarp (Chen et al., 2021), and *UFGT* and *F3H* were also found to be involved in the regulation of yellow cucumber (Wang LY et al., 2020). Wu et al. (2020) found that *CHS* and *DFR* genes were beneficial to the formation of the yellow leaves of ginkgo. Genes *CHI*, *F3H*, *F3'H*, *FLS*, and *ANS* were highly expressed in the yellow celery, and hence might contribute to the yellow color of celery.

Overall, the expression of abundant genes and metabolites in pigment biosynthesis pathways can directly influence pigment accumulation, thereby determining the color of plant tissues. In addition, variation in metabolites contributes to the nutritional quality of different cultivars. For example, metabolites with promising health effects such as apigenin and catechin were found to be significantly enriched in the green celery. The most abundant metabolites identified in the present study not only provide information for the enhancement of biological activities in celery, but also offer a valuable reference for mining metabolites in plants of different colors.

Acknowledgments

This work was supported by the National Natural Science Foundation of China (No. 32002027).

Author contributions

Conceptualization: Mengyao LI and Haoru TANG; Data curation: Jie LI, Ya LUO, Yong ZHANG, and Yan WANG; Formal analysis: Haohan TAN and Yunting ZHANG; Investigation: Yuanxiu LIN, Qing CHEN, and Haohan TAN; Writing-original draft: Mengyao LI and Jie LI; Writing-editing: Xiaorong WANG. All authors have read and approved the final manuscript, and therefore, have full access to all the data in the study and take responsibility for the integrity and security of the data.

Compliance with ethics guidelines

Mengyao LI, Jie LI, Haohan TAN, Ya LUO, Yong ZHANG, Qing CHEN, Yan WANG, Yuanxiu LIN, Yunting ZHANG, Xiaorong WANG, and Haoru TANG declare that they have no conflict of interest.

This article does not contain any studies with human or animal subjects performed by any of the authors.

References

Beale SI, 2005. Green genes gleaned. *Trends Plant Sci*, 10(7): 309-312.
https://doi.org/10.1016/j.tplants.2005.05.005

Chen C, Zhou G, Chen J, et al., 2021. Integrated metabolome and transcriptome analysis unveils novel pathway involved in the formation of yellow peel in cucumber. *Int J Mol Sci*, 22(3):1494.
https://doi.org/10.3390/ijms22031494

Cotter D, Maer A, Guda C, et al., 2006. LMPD: LIPID MAPS proteome database. *Nucleic Acids Res*, 34(S1): D507-D510.
https://doi.org/10.1093/nar/gkj122

Dong T, Han RP, Yu JW, et al., 2019. Anthocyanins accumulation and molecular analysis of correlated genes by metabolome and transcriptome in green and purple asparaguses (*Asparagus officinalis*, L.). *Food Chem*, 271:18-28.
https://doi.org/10.1016/j.foodchem.2018.07.120

Eckhardt U, Grimm B, Hörtensteiner S, 2004. Recent advances in chlorophyll biosynthesis and breakdown in higher plants. *Plant Mol Biol*, 56(1):1-14.
https://doi.org/10.1007/s11103-004-2331-3

Feng K, Liu JX, Xing GM, et al., 2019. Selection of appropriate reference genes for RT-qPCR analysis under abiotic stress and hormone treatment in celery. *PeerJ*, 7: e7925.
https://doi.org/10.7717/peerj.7925

Fenger JA, Roux H, Robbins RJ, et al., 2021. The influence

of phenolic acyl groups on the color of purple sweet potato anthocyanins and their metal complexes. *Dyes Pigments*, 185:108792. https://doi.org/10.1016/J.DYEPIG.2020.108792

Ferreyra MLF, Rius SP, Casati P, 2012. Flavonoids: biosynthesis, biological functions, and biotechnological applications. *Front Plant Sci*, 3:222. https://doi.org/10.3389/fpls.2012.00222

Fiehn O, 2002. Metabolomics—the link between genotypes and phenotypes. *Plant Mol Biol*, 48(1-2):155-171. https://doi.org/10.1023/A:1013713905833

Grotewold E, 2006. The genetics and biochemistry of floral pigments. *Annu Rev Plant Biol*, 57:761-780. https://doi.org/10.1146/annurev.arplant.57.032905.105248

Han XY, Luo YT, Lin JY, et al., 2021. Generation of purple-violet chrysanthemums via anthocyanin B-ring hydroxylation and glucosylation introduced from *Osteospermum hybrid F3'5'H* and *Clitoria ternatea A3'5'GT*. *Ornament Plant Res*, 1:4. https://doi.org/10.48130/OPR-2021-0004

Jan R, Asaf S, Paudel S, et al., 2021. Discovery and validation of a novel step catalyzed by *OsF3H* in the flavonoid biosynthesis pathway. *Biology*, 10(1):32. https://doi.org/10.3390/biology10010032

Jewett MC, Hofmann G, Nielsen J, 2006. Fungal metabolite analysis in genomics and phenomics. *Curr Opin Biotechnol*, 17(2):191-197. https://doi.org/10.1016/j.copbio.2006.02.001

Jia LD, Wang JS, Wang R, et al., 2021. Comparative transcriptomic and metabolomic analyses of carotenoid biosynthesis reveal the basis of white petal color in *Brassica napus*. *Planta*, 253:8. https://doi.org/10.1007/s00425-020-03536-6

Jiang SK, Zhang XJ, Xu ZJ, et al., 2010. Comparison between QTLs for chlorophyll content and genes controlling chlorophyll biosynthesis and degradation in *Japonica* rice. *Acta Agronom Sin*, 36(3):376-384. https://doi.org/10.1016/S1875-2780(09)60036-5

Li MY, Hou XL, Wang F, et al., 2018. Advances in the research of celery, an important Apiaceae vegetable crop. *Crit Rev Biotechnol*, 38(2):172-183. https://doi.org/10.1080/07388551.2017.1312275

Li SP, Deng BL, Tian S, et al., 2021. Metabolic and transcriptomic analyses reveal different metabolite biosynthesis profiles between leaf buds and mature leaves in *Ziziphus jujuba* Mill. *Food Chem*, 347:129005. https://doi.org/10.1016/j.foodchem.2021.129005

Li XB, Wang Y, Jin L, et al., 2021. Development of fruit color in *Rubus chingii* Hu (Chinese raspberry): a story about novel offshoots of anthocyanin and carotenoid biosynthesis. *Plant Sci*, 311:110996. https://doi.org/10.1016/j.plantsci.2021.110996

Liu HN, Su J, Zhu YF, et al., 2019. The involvement of *PybZIPa* in light-induced anthocyanin accumulation via the activation of *PyUFGT* through binding to tandem G-boxes in its promoter. *Hortic Res*, 6:134. https://doi.org/10.1038/s41438-019-0217-4

Liu Y, Tikunov Y, Schouten RE, et al., 2018. Anthocyanin biosynthesis and degradation mechanisms in *Solanaceous* vegetables: a review. *Front Chem*, 6:52. https://doi.org/10.3389/fchem.2018.00052

Liu Y, Shao YR, Li XY, et al., 2020. Analysis of nicotine-induced metabolic changes in *Blakeslea trispora* by GC-MS. *J Zhejiang Univ-Sci B (Biomed & Biotechnol)*, 21(2):172-177. https://doi.org/10.1631/jzus.B1900459

Ma Y, Feng YH, Diao TW, et al., 2020. Experimental and theoretical study on antioxidant activity of the four anthocyanins. *J Mol Struct*, 1204:27509. https://doi.org/10.1016/j.molstruc.2019.127509

Masoudi-Nejad A, Goto S, Jauregui R, et al., 2007. EGENES: transcriptome-based plant database of genes with metabolic pathway information and expressed sequence tag indices in KEGG. *Plant Physiol*, 144(2):857-866. https://doi.org/10.1104/pp.106.095059

Nagella P, Ahmad A, Kim SJ, et al., 2012. Chemical composition, antioxidant activity and larvicidal effects of essential oil from leaves of *Apium graveolens*. *Immunopharm Immunot*, 34(2):205-209. https://doi.org/10.3109/08923973.2011.592534

Nakabayashi R, Yonekura-Sakakibara K, Urano K, et al., 2014. Enhancement of oxidative and drought tolerance in Arabidopsis by overaccumulation of antioxidant flavonoids. *Plant J*, 77(3):367-379. https://doi.org/10.1111/tpj.12388

Oliver MJ, Guo LN, Alexander DC, et al., 2011. A sister group contrast using untargeted global metabolomic analysis delineates the biochemical regulation underlying desiccation tolerance in *Sporobolus stapfianus*. *Plant Cell*, 23(4):1231-1248. https://doi.org/10.1105/tpc.110.082800

Patil RH, Babu RL, Naveen KM, et al., 2015. Apigenin inhibits PMA-induced expression of pro-inflammatory cytokines and AP-1 factors in A549 cells. *Mol Cell Biochem*, 403(1-2):95-106. https://doi.org/10.1007/s11010-015-2340-3

Peng YY, Lin-Wang K, Cooney JM, et al., 2019. Differential regulation of the anthocyanin profile in purple kiwifruit (*Actinidia species*). *Hortic Res*, 6:3. https://doi.org/10.1038/s41438-018-0076-4

Pfaffl MW, 2001. A new mathematical model for relative quantification in real-time RT-PCR. *Nucleic Acids Res*, 29(9):e45. https://doi.org/10.1093/nar/29.9.e45

Shi QQ, Du JT, Zhu DJ, et al., 2020. Metabolomic and transcriptomic analyses of anthocyanin biosynthesis mechanisms in the color mutant *Ziziphus jujuba* cv. Tailihong. *J Agric Food Chem*, 68(51):15186-15198. https://doi.org/10.1021/acs.jafc.0c05334

Song XM, Sun PC, Yuan JQ, et al., 2021. The celery genome sequence reveals sequential paleo-polyploidizations, karyotype evolution and resistance gene reduction in apiales. *Plant Biotechnol J*, 19(4):731-744. https://doi.org/10.1111/pbi.13499

Sowbhagya HB, 2014. Chemistry, technology, and nutraceutical functions of celery (*Apium graveolens* L.): an overview.

Crit Rev Food Sci Nutr, 54(3):389-398. https://doi.org/10.1080/10408398.2011.586740

Sun TH, Yuan H, Cao HB, et al., 2018. Carotenoid metabolism in plants: the role of plastids. *Mol Plant*, 11(1):58-74. https://doi.org/10.1016/j.molp.2017.09.010

Tan GF, Ma J, Zhang XY, et al., 2017. *AgFNS* overexpression increase apigenin and decrease anthocyanins in petioles of transgenic celery. *Plant Sci*, 263:31-38. https://doi.org/10.1016/j.plantsci.2017.07.001

Wang LY, Tian YC, Shi W, et al., 2020. The miR396-GRFs module mediates the prevention of photo-oxidative damage by brassinosteroids during seedling de-etiolation in Arabidopsis. *Plant Cell*, 32(8):2525-2542. https://doi.org/10.1105/tpc.20.00057

Wang M, Chen L, Liang ZJ, et al., 2020. Metabolome and transcriptome analyses reveal chlorophyll and anthocyanin metabolism pathway associated with cucumber fruit skin color. *BMC Plant Biol*, 20:386. https://doi.org/10.1186/s12870-020-02597-9

Want EJ, Masson P, Michopoulos F, et al., 2013. Global metabolic profiling of animal and human tissues via UPLC-MS. *Nat Protoc*, 8(1):17-32. https://doi.org/10.1038/nprot.2012.135

Wei K, Zhang YZ, Wu LY, et al., 2016. Gene expression analysis of bud and leaf color in tea. *Plant Physiol Biochem*, 107:310-318. https://doi.org/10.1016/j.plaphy.2016.06.022

Wen B, Mei ZL, Zeng CW, et al., 2017. metaX: a flexible and comprehensive software for processing metabolomics data. *BMC Bioinformatics*, 18:183. https://doi.org/10.1186/s12859-017-1579-y

Wishart DS, Tzur D, Knox C, et al., 2007. HMDB: the human metabolome database. *Nucleic Acids Res*, 35(S1):D521-D526. https://doi.org/10.1093/nar/gkl923

Wu YQ, Guo J, Wang TL, et al., 2020. Metabolomic and transcriptomic analyses of mutant yellow leaves provide insights into pigment synthesis and metabolism in *Ginkgo biloba*. *BMC Genomics*, 21:858. https://doi.org/10.1186/s12864-020-07259-6

Xia Y, Chen WW, Xiang WB, et al., 2021. Integrated metabolic profiling and transcriptome analysis of pigment accumulation in *Lonicera japonica* flower petals during colour-transition. *BMC Plant Biol*, 21:98. https://doi.org/10.1186/s12870-021-02877-y

Xu ZS, Yang QQ, Feng K, et al., 2020. DcMYB113, a root-specific R2R3-MYB, conditions anthocyanin biosynthesis and modification in carrot. *Plant Biotechnol J*, 18(7):1585-1597. https://doi.org/10.1111/pbi.13325

Zeng ZQ, Lin TZ, Zhao JY, et al., 2020. *OsHemA* gene, encoding glutamyl-tRNA reductase (GluTR) is essential for chlorophyll biosynthesis in rice (O*ryza sativa*). *J Integr Agr*, 19(3):612-623. https://doi.org/10.1016/S2095-3119(19)62710-3

Zhang LY, Yu YB, Yu RZ, 2020. Analysis of metabolites and metabolic pathways in three maize (*Zea mays* L.) varieties from the same origin using GC-MS. *Sci Rep*, 10:17990. https://doi.org/10.1038/s41598-020-73041-z

Zhang WJ, Liu C, Yang RJ, et al., 2019. Comparison of volatile profiles and bioactive components of sun-dried Pu-erh tea leaves from ancient tea plants on Bulang Mountain measured by GC-MS and HPLC. *J Zhejiang Univ-Sci B (Biomed & Biotechnol)*, 20(7):563-575. https://doi.org/10.1631/jzus.B1800183

Zhou DD, Li R, Zhang H, et al., 2020. Hot air and UV-C treatments promote anthocyanin accumulation in peach fruit through their regulations of sugars and organic acids. *Food Chem*, 309:125726. https://doi.org/10.1016/j.foodchem.2019.125726

Zhu T, Wang X, Xu ZM, et al., 2020. Screening of key genes responsible for *Pennisetum setaceum* 'Rubrum' leaf color using transcriptome sequencing. *PLoS ONE*, 15(11):e0242618. https://doi.org/10.1371/journal.pone.0242618

Supplementary information

Tables S1–S5; Figs. S1 and S2